Table 3. Virus titers in the tissues of ducks infected with Ck/Yamaguchi/04 (H5N1) or Dk/Yokohama/03 (H5N1)

	Ck/Yamaguchi/04 (H5N1)						Dk/Yokohama/03 (H5N1)					
	Virus titer[a] in the following tissues						Virus titer[a] in the following tissues					
Days p.i.	Trachea and Lungs	Liver	Kidneys	Colon	Brain	Blood	Trachea and Lungs	Liver	Kidneys	Colon	Brain	Blood
1	–[b]	–	–	–	–	–	3.3	2.5	–	–	–	≤1.3
2	6.5	–	3.7	≤2.3	–	–	6.7	3.5	5.7	3.3	2.5	1.5
	4.7	3.5	5.5	4.5	–	≤1.3	7.3	2.5	5.5	5.7	–	≤0.7
3	5.7	3.5	–	3.5	2.5	–	6.3	2.5	5.7	–	–	–
	7.5	3.5	7.5	6.5	–	≤1.3	6.5	4.3	6.7	3.7	3.3	1.5
4	6.5	4.5	5.3	5.5	–	–	6.3	–	4.7	–	6.5[c]	–
	5.5	–	–	–	–	–	6.3	≤2.3	5.3	–	–	–
5	4.5	–	–	–	–	–	5.5	3.7	4.5	3.5	6.5[c]	–
	5.3	–	3.5	2.7	–	–	6.5	3.7	5.5	5.5	2.7	1.7
6	3.5	–	4.5	–	–	–	–	–	–	–	–	–
7	–	–	2.7	2.5	–	–	–	–	–	–	–	–

[a]Organs: log EID_{50}/g, Blood: log EID_{50}/ml
[b]<1.5 log EID_{50}/g in organs, <0.5 log EID_{50}/ml in blood
[c]Before sacrifice for organ collection, the duck showed neurological signs such as headshaking and blindness

at high titers in the brains of the ducks on days 4 and 5 p.i. The ducks with high titers of virus detected in the brain showed neurological signs such as headshake and blindness when euthanized to collect the organs. Virus was recovered from the blood of 5 ducks infected with Dk/Yokohama/03 and of 2 ducks infected with Ck/Yamaguchi/04.

In the histopathological analysis, infection with Dk/Yokohama/03 was found to have produced lesions in the brains and hearts of infected ducks which showed neurological signs. The microscopic lesion of the brain was severe virus encephalitis with the histopathological findings as mentioned above. Influenza virus antigens were detected in nerve cells and neuroglia cells (Fig. 1). The microscopic lesion of the heart was myocarditis with multifocal degeneration and necrosis

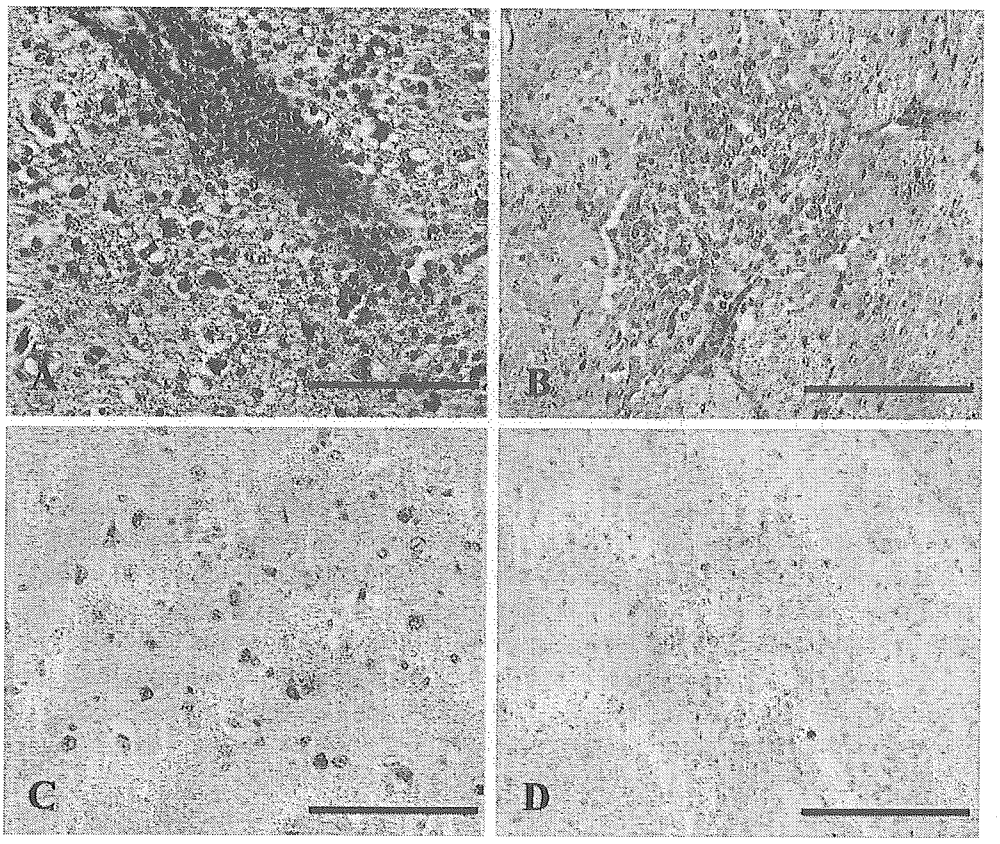

Fig. 1. Experiments in ducks infected with Dk/Yokohama/03 on day 5 p.i. Photomicrographs of hematoxylin and eosin-stained tissue sections (**A** and **B**) and photomicrographs of tissue sections stained immunohistochemically to demonstrate viral antigens (**C** and **D**). **A**: Perivascular cuffing, edema, swelling of endothelial cells, infiltration and proliferation of microglia, and degeneration and necrosis of nerve cells. **B**: Viral antigens in nerve cells and neuroglia cells. **C**: Myocarditis with multifocal degeneration and necrosis of myocytes, and infiltration of macrophages and heterophils. **D**: Viral antigens in myocytes. Bar, 100 μm

of myocytes, and infiltration of macrophages and heterophils. Influenza virus antigens were detected in cardiac myocytes (Fig. 1). The bursa of the ducks infected with Dk/Yokohama/03 showed signs of mild lymphoid follicular hyperplasia with a few fragmented nuclei of lymphoid cells in the medulla from 2 to 7 days p.i. These changes were most prominent at 3, 4 and 5 days p.i.

Infection with Ck/Yamaguchi/04 was found to have produced less severe lesions than infection with Dk/Yokohama/03 in the brains, hearts and bursa of infected ducks. The microscopic lesions were mild perivascular cuffing in the brain and mild infiltration of lymphocytes and macrophages in the heart at 5 day p.i. In the other organs infected with each of the strains, such as the trachea, lungs, kidneys, liver, pancreas and colon, no histopathological signs were observed.

These results indicate that Dk/Yokohama/03 replicates more rapidly and efficiently than Ck/Yamaguchi/04 in ducks.

Discussion

Ck/Yamaguchi/04, Dk/Yokohama/03, HK/483/97 and Tn/SA/61 used in the present study are highly pathogenic for chickens. The ducks infected with HK/483/97 and Tn/SA/61 did not show any clinical signs and virus was recovered only from a limited number of organs such as the respiratory tract, kidneys and colon. In contrast, Ck/Yamaguchi/04 and Dk/Yokohama/03 were recovered from multiple organs of the infected ducks. There was an obvious difference between these strains in that the ducks infected with Ck/Yamaguchi/04 did not show overt signs, whereas those infected with Dk/Yokohama/03 showed neurological signs although none of them died. These results indicate that the highly pathogenic avian influenza viruses vary in pathogenicity for ducks. These results are consistent with those of Sturm-Ramirez et al. [10]. The result that Dk/Yokohama/03 is more virulent in ducks than Ck/Yamaguchi/04 indicates that the most recent HPAI H5 strain is not necessarily more pathogenic for ducks. Considering that Ck/Yamaguchi/04 was more pathogenic than Dk/Yokohama/03 in chickens (data not shown), Ck/Yamaguchi/04 may have adapted to chickens and Dk/Yokohama/03 may have adapted to ducks, respectively.

None of the ducks infected with Ck/Yamaguchi/04 or Dk/Yokohama/03 died. The ducks infected with Ck/Yamaguchi/04 did not even show any clinical signs. However, in the field, environmental factors may affect the infection with influenza virus. We have shown that influenza virus infection may be exacerbated by the co-infection of bacteria in the field [6]. The blind duck cannot eat and may die in the field. If ducks are infected with Ck/Yamaguchi/04 and Dk/Yokohama/03 in the field, they may show more severe clinical signs or even die.

Tanaka et al. [12] showed that HK/483/97 reaches the brain through the nerves in mice as the virus was detected in the trigeminal and vagal ganglia even though no virus was recovered from the blood of these mice. On the other hand, virus was recovered from the blood of infected chickens. Ck/Yamaguchi/04 and Dk/Yokohama/03 may reach the brain through the blood as these viruses

were recovered from the blood of the infected ducks during the early period of infection.

The ducks infected with Dk/Yokohama/03 showed neurological signs while those infected with Ck/Yamaguchi/04 did not show any clinical signs. Regarding their growth kinetics, Dk/Yokohama/03 was recovered efficiently from the brain of the infected ducks although Ck/Yamaguchi/04 was recovered at low titers from the brain of only one of the ducks infected. The virus titers of the brains of the ducks infected with Dk/Yokohama/03 that showed neurological signs were high (6.5 EID_{50}/g). However, the titers of the brains of the ducks infected with Dk/Yokohama/03, that did not show any clinical signs, were low (2.5 to 3.3 EID_{50}/g). The peak in growth of Dk/Yokohama/03 in the brain of the ducks was on day 4 or 5 p.i. Concomitantly, the infected ducks also began to show neurological signs on day 4 or 5 p.i. These results indicate that the viral growth in the brain affects the central nervous system and causes neurological signs in ducks. Dk/Yokohama/03 caused a faster systemic infection than Ck/Yamaguchi/04 in ducks. Dk/Yokohama/03, therefore, may escape from the immune response of the host and be able to grow fully in the brain of the ducks and cause neurological dysfunction. Dk/Yokohama/03 produced myocarditis with multifocal degeneration and necrosis of myocytes in the heart of the ducks infected with the virus on days 4 and 5 p.i. The myocarditis was mild although a more severe form would lead to death. Why is it that Ck/Yamaguchi/04 caused little damage to the tissues of infected ducks and did not cause death in ducks as it did in chickens although high titers of virus were detected in multiple organs? Further studies are required to investigate the mechanism involved.

Ck/Yamaguchi/04 grows in multiple organs of ducks lacking overt signs, although virus shedding from the infected ducks lasts only for about one week. If the ducks infected with HPAIV do not show any signs as was case with those infected with Ck/Yamaguchi/04, it would be difficult to detect infections at early stages, paving the way for an epidemic of HPAI. It is, therefore, important to carry out constant surveillance of avian influenza in domestic ducks on farms and live bird markets.

Acknowledgments

We thank A. S. Mweene for critical reviews of the manuscript. This study was supported by Grants-in-Aid for Scientific Research 15108004 from the Ministry of Education, Science, Culture and Sports, Japan.

References

1. Alexander DJ, Allan WH, Parsons DG, Parsons G (1978) The pathogenicity of four avian influenza viruses for fowls, turkeys and ducks. Res Vet Sci 24: 242–247
2. Alexander DJ (2000) A review of avian influenza in different bird species. Vet Microbiol 74: 3–13
3. Cauthen AN, Swayne DE, Schultz-Cherry S, Perdue ML, Suarez DL (2000) Continued circulation in China of highly pathogenic avian influenza viruses encoding the

hemagglutinin gene associated with the 1997 H5N1 outbreak in poultry and humans. J Virol 74: 6592–6599
4. Easterday BC, Hinshow VS, Halvorson DA (1997) Influenza. In: Calnec BW (ed) Diseases of poultry, 10th ed. Iowa State University Press, Ames, IA, pp 583–605
5. Kida H, Webster RG, Yanagawa R (1983) Inhibition of virus-induced hemolysis with monoclonal antibodies to different antigenic areas on the hemagglutinin molecule of A/seal/Massachusetts/1/80 (H7N7) influenza virus. Arch Virol 76: 91–99
6. Kishida N, Sakoda Y, Eto M, Sunaga Y, Kida H (2004) Co-infection of Staphylococcus aureus or Haemophilus paragallinarum exacerbates H9N2 influenza A virus infection in chickens. Arch Virol 149: 2095–2104
7. Perkins LE, Swayne DE (2002) Pathogenicity of a Hong Kong-origin H5N1 highly pathogenic avian influenza virus for emus, geese, ducks, and pigeons. Avian Dis 46: 53–63
8. Reed LJ, Muench H (1938) A simple method for estimating fifty percent endpoints. Am J Hyg 37: 493–497
9. Shortridge KF, Zhou NN, Guan Y, Gao P, Ito T, Kawaoka Y, Kodihalli S, Krauss S, Markwell D, Murti KG, Norwood M, Senne D, Sims L, Takada A, Webster RG (1998) Characterization of avian H5N1 influenza viruses from poultry in Hong Kong. Virology 252: 331–342
10. Sturm-Ramirez KM, Ellis T, Bousfield B, Bissett L, Dyrting K, Rehg JE, Poon L, Guan Y, Peiris M, Webster RG (2004) Reemerging H5N1 influenza viruses in Hong Kong in 2002 are highly pathogenic to ducks. J Virol 78: 4892–4901
11. Sugimura T, Ogawa T, Tanaka Y, Kumagai T (1981) Antigenic type of fowl plague virus isolated in Japan in 1925. Natl Inst Anim Health Q (Tokyo) 21: 104–105
12. Tanaka H, Park CH, Ninomiya A, Ozaki H, Takada A, Umemura T, Kida H (2003) Neurotropism of the 1997 Hong Kong H5N1 influenza virus in mice. Vet Microbiol 95: 1–13
13. Tumpey TM, Suarez DL, Perkins LE, Senne DA, Lee JG, Lee YJ, Mo IP, Sung HW, Swayne DE (2002) Characterization of a highly pathogenic H5N1 avian influenza A virus isolated from duck meat. J Virol 76: 6344–6355
14. Webster RG, Guan Y, Peiris M, Walker D, Krauss S, Zhou NN, Govorkova EA, Ellis TM, Dyrting KC, Sit T, Perez DR, Shortridge KF (2002) Characterization of H5N1 influenza viruses that continue to circulate in geese in southeastern China. J Virol 76: 118–126
15. Yuen KY, Chan PK, Peiris M, Tsang DN, Que TL, Shortridge KF, Cheung PT, To WK, Ho ET, Sung R, Cheng AF (1998) Clinical features and rapid viral diagnosis of human disease associated with avian influenza A H5N1 virus. Lancet 351: 467–471

Author's address: Prof. Hiroshi Kida, Laboratory of Microbiology, Department of Disease Control, Graduate School of Veterinary Medicine, Hokkaido University, Sapporo, Hokkaido 060-0818, Japan; e-mail: kida@vetmed.hokudai.ac.jp

Journal of General Virology (2005), 86, 1131–1139 DOI 10.1099/vir.0.80704-0

In vitro demonstration of neural transmission of avian influenza A virus

Kazuya Matsuda,[1] Takuma Shibata,[1] Yoshihiro Sakoda,[2] Hiroshi Kida,[2] Takashi Kimura,[1] Kenji Ochiai[1] and Takashi Umemura[1]

Laboratory of Comparative Pathology[1], and Laboratory of Microbiology[2], Graduate School of Veterinary Medicine, Hokkaido University, Sapporo 060-0818, Japan

Correspondence
Takashi Umemura
umemura@vetmed.hokudai.ac.jp

Received 19 October 2004
Accepted 6 January 2005

Neural involvement following infections of influenza viruses can be serious. The neural transport of influenza viruses from the periphery to the central nervous system has been indicated by using mouse models. However, no direct evidence for neuronal infection has been obtained *in vitro* and the mechanisms of neural transmission of influenza viruses have not been reported. In this study, the transneural transmission of a neurotropic influenza A virus was examined using compartmentalized cultures of neurons from mouse dorsal root ganglia, and the results were compared with those obtained using the pseudorabies virus, a virus with well-established neurotransmission. Both viruses reached the cell bodies of the neurons via the axons. This is the first report on axonal transport of influenza A virus *in vitro*. In addition, the role of the cytoskeleton (microtubules, microfilaments and intermediate filaments) in the neural transmission of influenza virus was investigated by conducting cytoskeletal perturbation experiments. The results indicated that the transport of avian influenza A virus in the neurons was independent of microtubule integrity but was dependent on the integrity of intermediate filaments, whereas pseudorabies virus needed both for neural spread.

INTRODUCTION

Influenza A viruses belong to the family *Orthomyxoviridae* and contain eight single-stranded, negative-sense RNA segments that encode 10 polypeptides. Influenza A viruses are divided into subtypes on the basis of serological and genetic differences in their surface glycoproteins, haemagglutinin and neuraminidase, and the genes that encode them. Fifteen subtypes of haemagglutinin and nine subtypes of neuraminidase have been identified and all can be obtained from their natural hosts, water fowl and shore birds (Kida *et al.*, 1980, 1987; Webster *et al.*, 1992). Most influenza infections in humans cause upper respiratory tract disorders, but the other organs including the lungs, heart, liver, kidneys, muscles and brain can also be affected (Turner *et al.*, 2003). Central nervous system (CNS) involvements can be fatal particularly in infants and children (Togashi *et al.*, 1997), or pregnant women (Hakoda & Nakatani, 2000). Influenza A viruses or their genomes have been detected in cerebrospinal fluid (Hakoda & Nakatani, 2000; Togashi *et al.*, 1997) and viral proteins have been found in brain tissues (Frankova *et al.*, 1977).

In the 20th century, many influenza epidemics and pandemics have been caused by H1N1, H2N2 and H3N2 viruses. From 1997, H5N1 infections occurred in Asian countries and resulted in high mortality (Centers for Disease Control & Prevention, 2004; Tran *et al.*, 2004; Yuen *et al.*, 1998). Although it is thought that these viruses were derived directly from avian species, and person-to-person spreads were rare and inefficient (Claas *et al.*, 1998; Mounts *et al.*, 1999). The emergence of H5 viruses in humans has proved that avian influenza viruses can cross the host species barrier and warns of the threat of the pandemic of new human influenza A viruses resulting from the mutation or reassortment of human influenza viruses with co-infecting avian influenza A viruses.

Previously, we have established mouse models in which intranasally inoculated H5 influenza A viruses afferently infected the CNS via transneural routes (Matsuda *et al.*, 2004; Park *et al.*, 2002; Shinya *et al.*, 1998, 2000; Tanaka *et al.*, 2003). Here, we demonstrate retrograde axonal transport of a neurotropic H5 influenza virus using neurons in a compartmentalized culture system, and evaluate the effects on viral spread in the presence of drugs interfering with microtubules (MTs), microfilaments (MFs) and intermediate filaments (IFs), making comparisons with pseudorabies virus, a neurotropic alphaherpesvirus which can propagate transaxonally *in vitro* and *in vivo* (Card *et al.*, 1990; Enquist *et al.*, 2002; Field & Hill, 1974).

METHODS

Viruses. Avian influenza virus strain 24a5b (AIV), a highly pathogenic strain, was obtained from the avirulent strain A/whistling swan/Shimane/499/83 (H5N3) after 24 consecutive passages in the

air sacs of chicks and five passages in the brain of chicks; and has a serial basic amino acid sequence at the haemagglutinin cleavage site (Ito *et al.*, 2001). AIV exhibits marked pathogenicity in chicks (100 % mortality for 3-day-old chicks on air sac infection) (Silvano *et al.*, 1997) and neuropathogenicity in mice on intranasal inoculation (Matsuda *et al.*, 2004; Shinya *et al.*, 1998, 2000). This virus does not cause any pathological changes due to haematogenous viral spread in mice (Shinya *et al.*, 2000). AIV was propagated in the allantoic cavities of 10-day-old embryonated chicken eggs. All virus infection and incubation experiments were undertaken in the P3 biosafety area of our facility.

Pseudorabies virus, also known as Aujeszky's disease virus or suid herpes virus 1, belongs to the subfamily *Alphaherpesvirinae* of the family *Herpesviridae*. Pseudorabies virus strain Yamagata-S 81 (PRV) is the first Japanese isolate from piglets (Itakura *et al.*, 1981). This virus was propagated in cloned porcine kidney (CPK) cells.

Neuron culture. Sensory neurons from the dorsal root ganglia (DRG) of the spinal cord of newborn BALB/c mice (2–4 days old) were dissociated by incubation with 1 mg collagenase (Sigma-Aldrich) ml^{-1} at 37 °C for 30 min. Dissociated neurons were resuspended at a concentration of 40 000 neurons (about 80 ganglia) per ml in maintenance medium (MM) comprising Eagle's minimal essential medium (Sigma-Aldrich) supplemented with 10 % heat-inactivated fetal bovine serum (Sigma-Aldrich), 50 U penicillin (Invitrogen) ml^{-1} and 50 μg streptomycin (Invitrogen) ml^{-1}. Collagen-coated 35 mm dishes with a central 14 mm glass coverslip (Matsunami Glass) were seeded with 100 μl of the cell suspension. Cells were then incubated in MM with 10 μM 5-fluoro-2′-deoxyuridine (Sigma-Aldrich) and 40 nM 2·5S nerve growth factor (Invitrogen) in a 5 % CO_2 atmosphere at 37 °C. For the elimination of dividing cells, 6 μM aphidicolin (Sigma-Aldrich) was added to the medium from days 2 to 3 in addition to fluorodeoxyuridine. The medium was changed every 2–3 days. After 7–10 days of incubation, when an axonal network of neurons had formed, dishes were used for the experiments. At this time, over 1600 neurons survived in each dish and less than 3 % of all surviving cells were non-neuronal cells, i.e. Schwann cells and fibroblasts which were identified by morphology and immunocytochemistry (data not shown).

Infectious titre in neurons. To detect the infectious titre of stock viral suspensions in neurons, both AIV and PRV were diluted 10-fold in MM and overlaid on cultured neurons. After 60 h incubation in a 5 % CO_2 atmosphere at 37 °C, cells were screened for infectivity by immunofluorescent staining. Infectivity was calculated as 50 % neuronal tissue culture infective dose ($NTCID_{50}$). Neuronal infectious titres of stock suspensions of AIV were $10^{5.7}$ $NTCID_{50}$ ml^{-1}, which was $10^{7.5}$ 50 % egg infectious doses per ml, and that of PRV were $10^{7.1}$ $NTCID_{50}$ ml^{-1}, $10^{7.7}$ $TCID_{50}$ ml^{-1} in CPK cells, respectively.

Infection of neuronal cell bodies with AIV. Cultured neurons in the 14 mm coverslip were inoculated with AIV at an $NTCID_{50}$ of $10^{2.7}$ in 100 μl MM and incubated for 1 h at 37 °C. The viral suspension was removed and cells were washed three times with MM, then incubated in MM for 6, 12, 18, 24 and 36 h. At least three samples were examined for each time point. Mock-infected neurons were used as a negative control.

Compartmentalized neuron culture. The culture dishes for the compartmentalized culture system were prepared as follows (Fig. 1, Campenot, 1977; Campenot & Martin, 2001): 35 mm dishes with a central 27 mm glass coverslip (Matsunami Glass) were coated with collagen. Parallel scratches were made by fine needles on the coverslip. A drop of MM containing 0·4 % methyl cellulose was placed on the scratched region. A silicon divider (Shin-Etsu Chemical) with one end coated with a ribbon of silicon high vacuum grease (Dow Corning) was placed on the coverslip so that each chamber was sealed off. The wet surface of the scratched region with the medium prevented the silicon grease from adhering to the collagen, and neurons seeded in the central chamber could extend their axons to the side chambers through the gap between the silicon divider and collagen bed without any exchange of medium between the chambers. No leakage of the medium from the chambers was checked at each change of medium. Samples of resuspended cells (2000 neurons in 50 μl MM) were seeded into the central chamber. Growing axons penetrated under the divider walls and when the total number of axons in both chambers reached 20, each dish was used for viral inoculation. At this time, over 800 neurons survived in each central chamber and less than 3 % of all surviving cells were non-neuronal cells.

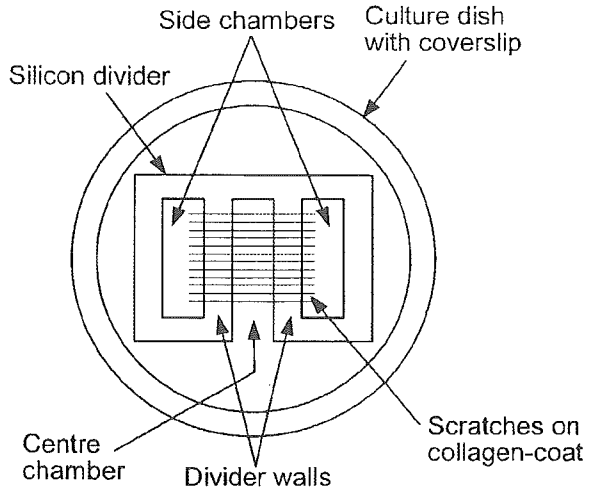

Fig. 1. Schematic diagram of a compartmentalized culture consisting of a silicon divider set on a 35 mm culture dish with a central 27 mm coverslip. A silicon divider with silicon high vacuum grease at the base is seated on a collagen-coated coverslip. Neurons seeded in the central chamber extend their axons along the scratches and reach the side chambers.

Inoculation of axons in compartmentalized culture system. We inoculated AIV or PRV into the axons of the side chambers. Before the inoculation, the culture medium of the central and side chambers was removed, and MM containing rabbit antiserum against each virus and 0·2 % methyl cellulose was added to the central chamber. Antiserum against influenza virus A/duck/Pennsylvania/10128/84 (H5N2) or against PRV (a gift from Dr Ono, Institute for Genetic Medicine, Hokkaido University, Japan) was used at a dilution of 1 : 20 for AIV and 1 : 50 for PRV. The antisera were used to neutralize viruses that leaked from the side chambers during absorption and extracellular viruses released from neurons. The concentrations of antiserum were enough to neutralize the viruses inoculated directly into the MM of the central chamber. For the viral infection of axons, AIV at an $NTCID_{50}$ of $10^{3.6}$ or PRV at an $NTCID_{50}$ of $10^{4.0}$ in 80 μl MM was inoculated in the side chambers and incubated for 1 h at 37 °C. The side chambers were then washed three times with MM and the medium was replaced with MM containing each antiserum and 0·2 % methyl cellulose. At 6, 12, 18, 24, 36, 48 and 60 h post-inoculation (p.i.), dishes were used for immunofluorescent staining. At least three dishes were examined for each virus and for each time point.

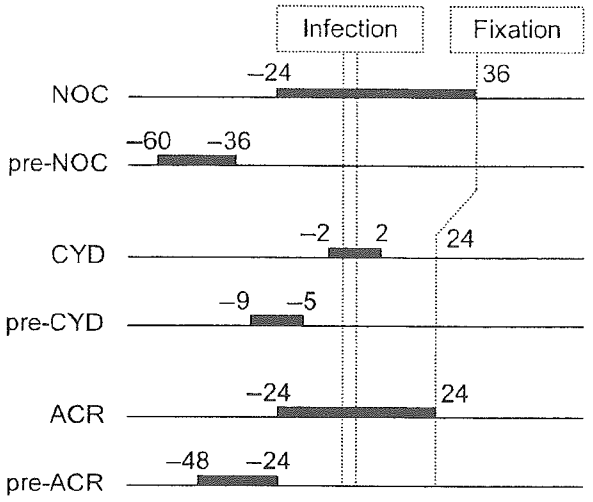

Fig. 2. Time schedule of drug treatment and viral infection. Neurons were infected with influenza virus strain 24a5b or pseudorabies virus strain Yamagata S-81 during or after drug treatment (filled bars on each cross line). Numbers represent hours before or after viral infection. NOC, Nocodazole; CYD, cytochalasin D; ACR, acrylamide.

Cytoskeletal interference and viral infection. Full-grown neurons with axonal networks were prepared on 14 mm coverslips on 35 mm dishes. Neurons pre-treated and recovered, or following treatment with 10 μM nocodazole (NOC; Sigma-Aldrich), 5 μM cytochalasin D (CYD; Sigma-Aldrich) or 4 mM acrylamide (ACR; Sigma-Aldrich), were inoculated with either AIV at an $NTCID_{50}$ of $10^{3.7}$ or PRV at an $NTCID_{50}$ of $10^{4.1}$ in 100 μl MM and incubated for 1 h at 37 °C (Fig. 2). The inoculum was then removed by washing with MM three times and MM was applied with or without each drug. NOC was used for the disruption of MTs, CYD for the disruption of MFs and ACR for the perturbation of IFs. Stock solutions of NOC (10 mM) in DMSO, CYD (1 mM) in DMSO and ACR (1 M) in double-distilled water were prepared and diluted to a final concentration in MM. The final concentrations were chosen to maximize the effect without any apparent morphological cytotoxicity (data not shown). Controls were treated with an equal volume of DMSO or double-distilled water. On the withdrawal of each drug, cells were washed with MM three times. At 24 or 36 h p.i., infected neurons were fixed for morphological examination. At least three dishes were used for each treatment. Student's *t*-test was used to assess the statistical significance of differences between the groups ($P<0{\cdot}01$).

Immunofluorescent staining and confocal laser scanning microscopy. Cells were fixed with 4% paraformaldehyde for 10 min and permeabilized with 0·2% Triton X-100 for 5 min. Non-specific binding of antibodies was blocked by incubation with 2% bovine serum albumin (Sigma-Aldrich) for 30 min. Rabbit antiserum against influenza virus A/duck/Pennsylvania/10128/84 (H5N2) or PRV was used for the detection of viral antigens. Monoclonal anti-tubulin βIII isoform antibody (Chemicon International), anti-neurofilament-M&H phosphorylated forms antibody (Chemicon International) and FITC-conjugated phalloidin (Sigma-Aldrich) were used to visualize MTs, neurofilaments (NFs) and MFs, respectively. FITC-conjugated anti-mouse IgG goat serum (Cooper Biomedical) and Alexa Fluor 555-conjugated anti-rabbit IgG donkey antiserum (Molecular Probes) were used as secondary antibodies. Hoechst 33258 (Wako Pure Chemical Industries) was used for nuclear staining. Analyses were performed with an Olympus Fluoview FV500 confocal laser scanning microscope and Fluoview software version 4.2. Infectivity was scored by counting over 400 neurons on the 14 mm coverslip or over 200 neurons in the central chamber of the compartmentalized culture system.

RESULTS

Infection of cultured neuron with AIV

To evaluate the infectivity of AIV, cultured neurons were directly inoculated with the virus. At 6 h p.i., viral antigens were present mostly in the nuclei of the neurons. After that, the perikarya and axons became positive. Axons connected with infected perikarya contained dotted viral antigens on tubulin (Fig. 3a, b). A few non-neuronal cells coexisting with the neurons were also infected. The percentage of infected neurons increased gradually with incubation time (Fig. 4). No severe damage, due to infection, was observed in the neurons except for a mild swelling of cell bodies.

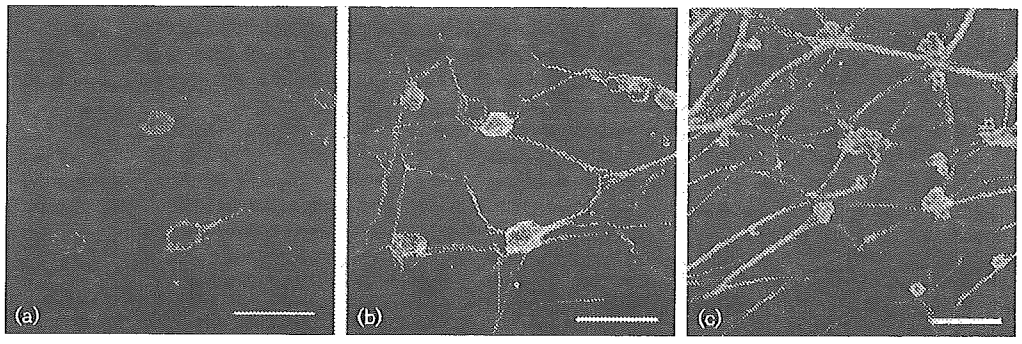

Fig. 3. Confocal images of neurons infected with influenza virus strain 24a5b and examined at 36 h p.i. (a, b) and mock-infected neurons (c). Cells were immunostained for virus antigen (a–c; red) and tubulin βIII (b, c; green). (a, b) Dots of viral antigens among cell bodies are overlaid on the axons stained for tubulin. (c) Viral antigens are absent. Bars, 50 μm (a, b); 100 μm (c).

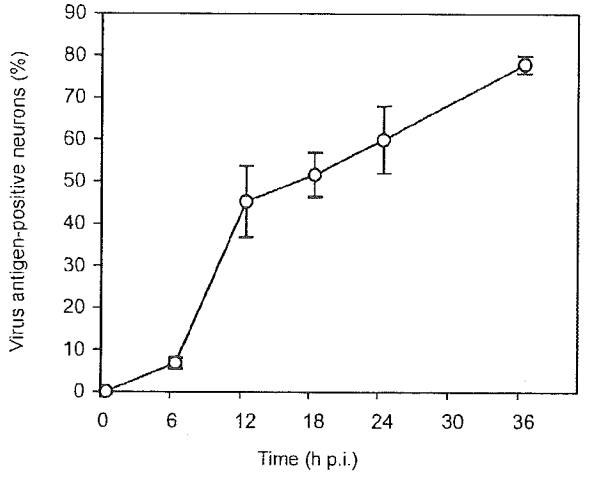

Fig. 4. Percentage of virus antigen-positive neurons after influenza virus strain 24a5b infection. Each value is expressed as the mean ± SD.

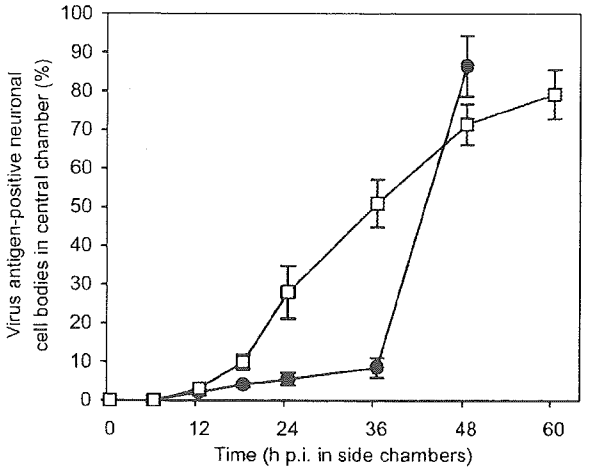

Fig. 5. Axonal transport of influenza and pseudorabies virus assayed in a compartmentalized culture system. Each value is expressed as the mean ± SD. At each time point over 200 neurons were examined for the antigens. □, Influenza virus strain 24a5b; ●, pseudorabies virus strain Yamagata S-81.

Neurons without virus infection showed no staining for viral antigens (Fig. 3c).

Axonal transport of AIV and PRV in compartmentalized culture system

To demonstrate the axonal transport of AIV and PRV in compartmentalized neuron culture, the viruses were allowed to infect the axons in the side chambers, and then the percentage of cell bodies positive for viral antigens in the central chamber was calculated. Both viral antigens first appeared in the neuronal cell bodies at 12 h p.i., and infected neurons increased afterwards for both viruses (Fig. 5). Taking into account of the fact that only a minority of the neurons extended their axons to the side chambers (20 axons of approx. 800 surviving neurons) and that neurons in the central chamber were connected by their processes, cell-to-cell spread of the viruses among the neurons must have occurred. The pattern of infection clearly differed between the viruses: the number of cells positive for AIV increased gradually, whereas the number of cells positive for PRV increased slowly until 36 h p.i. and then abruptly from 36 to 48 h p.i. Neurons infected with PRV showed a coarsely dotted pattern of staining for viral antigens, and collapsed and unstained neurons were observed more frequently than in AIV-infected cells. Although a small number of non-neuronal cells were also infected with AIV, infected neurons were rarely associated with such non-neuronal cells.

Effects of cytoskeletal perturbation caused by drug treatment on viral spread in cultured neurons

To compare the modes of axonal transport of the two viruses, cultured neurons disrupted selectively in the cytoskeleton, using inhibitors, were infected with the viruses. To ascertain that the adverse effects of the inhibitors on the cytoskeleton were reversible and did not kill the neurons, the infectivity of cultured neurons recovered from the drug treatment (pre-treated groups) was also compared with that of untreated control cells (schematically shown in Fig. 2). Confocal images of tubulin revealed granular to fibrillary staining in the cell bodies and fibrous staining in the untreated axons (Fig. 3b). NOC treatment strongly abated the tubulin staining and a few fine linear MTs were observed (Fig. 6b). Removal of NOC led to a re-emergence of the MTs (Fig. 6d). In the neurons treated or pre-treated with NOC, AIV spread decreased insignificantly, whereas PRV showed a 90 % reduction of axonal transport in the presence of NOC (Fig. 7a). This reduction was not observed in the neurons recovered from the drug treatment. Immunofluorescent dots of both viral antigens were enlarged in the NOC-treated axons (Figs 3a, 6a and c). The morphology of actin filaments was unaffected by CYD treatment (Fig. 6e), and the percentages of antigen-positive neurons were not significantly modified by the treatment for either virus (Fig. 7b). NFs exhibited fibrillary staining in the cell bodies and axons in the untreated neurons (Fig. 6h), and neurons after recovery. With the ACR treatment, NF protein characteristically accumulated at the axon terminals and viral antigens disappeared from the axons (Fig. 6f–h). In the ACR-treated neurons, the number of cells positive for AIV decreased to 68 % and that of cells positive for PRV decreased to 20 % of the untreated control (Fig. 7c). These decreasing proportions of the number of neurons positive for both viruses with the ACR treatment differed significantly. The neurons recovered from ACR treatment showed a similar infectivity

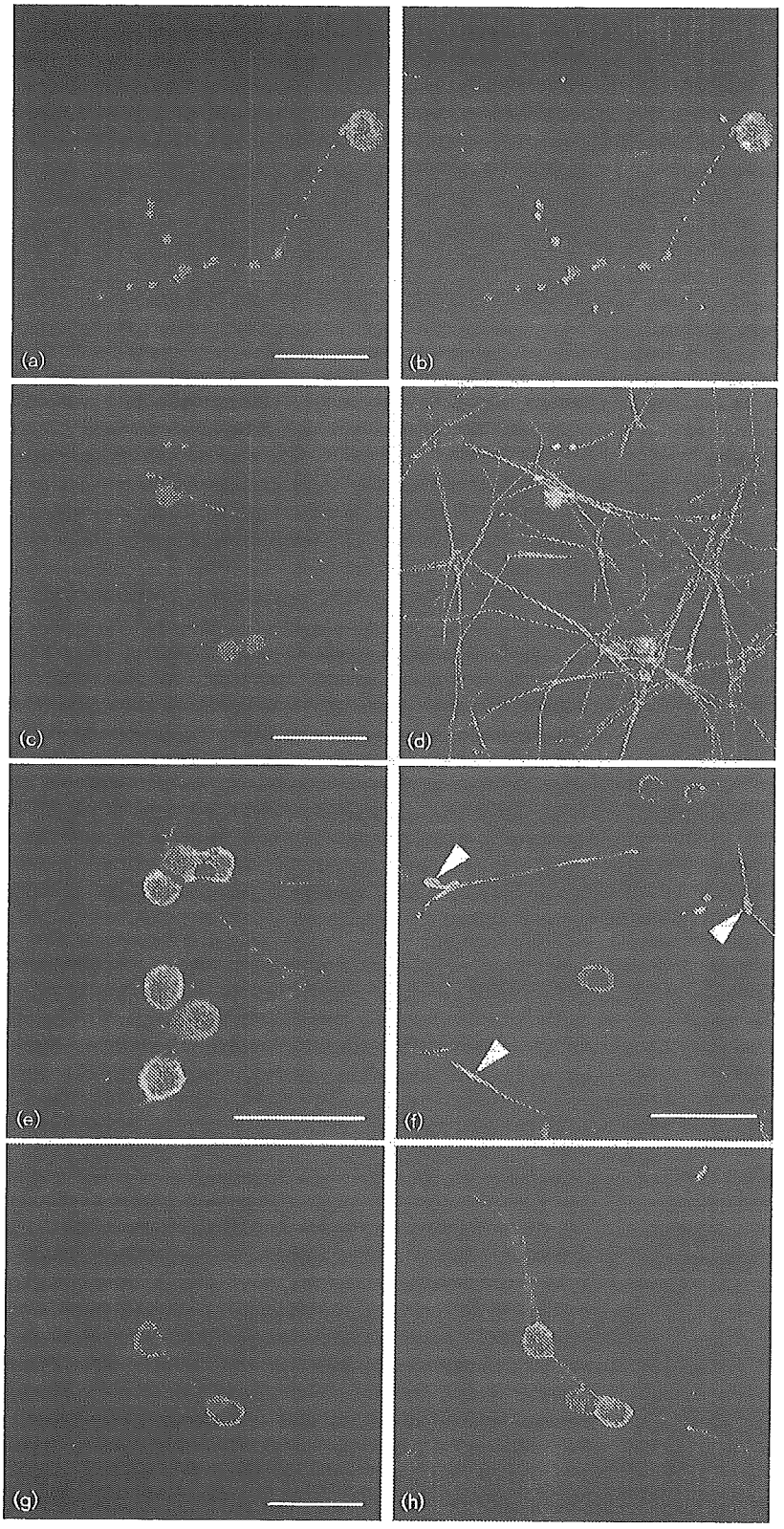

Fig. 6. Confocal images of neurons infected with influenza virus strain 24a5b with or without drug treatment. (a–d) Neurons were treated (a, b) or pre-treated (c, d) with NOC, then infected with the virus, and examined at 36 h p.i. Cells were immunostained for virus antigen (red) and tubulin βIII (b, d; green). Nuclei were stained with Hoecst 33258 (b, d; blue). (a, b) Enlargement of dotted viral antigens in comparison with those in untreated neurons shown in Fig. 3(a) and (b). Microtubules almost disappeared following the NOC treatment. (c, d) Pre-treated neurons were stained for the viral antigens similarly to the untreated neurons (Fig. 3a and b), and microtubules are reconstructed. (e) Neurons were treated with CYD, infected with strain 24a5b and examined at 24 h p.i. Diffuse staining for filamentous actin is not modified by the treatment (green). Virus antigens in the perikarya and axons (red). (f–h) Neurons treated with (f) or without (g, h) ACR, infected with the virus, and examined at 24 h p.i. (f) Arrowheads indicate accumulation of neurofilament proteins at the axon terminals (green). Viral antigens are absent in the axon (red). (g, h) Fibrillary staining for neurofilament proteins throughout the cell bodies and axons. Viral antigens are within the cell bodies and axons (red). Bars, 50 μm.

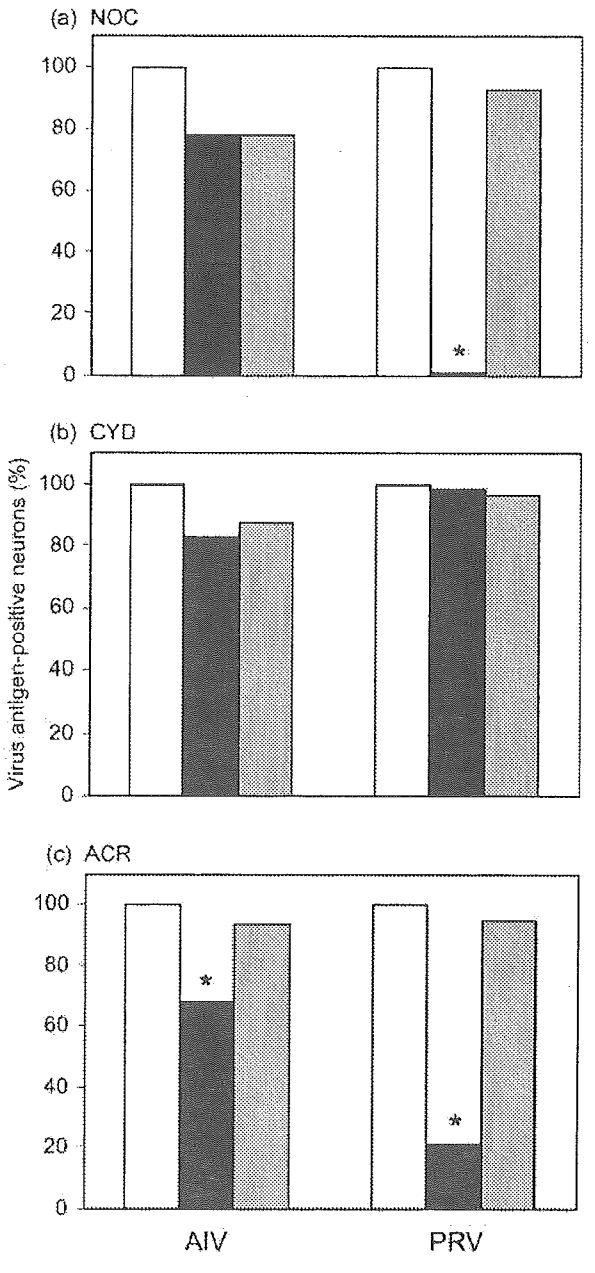

Fig. 7. Effects of cytoskeletal perturbation on viral spread in the neuronal network. Neurons were treated (black columns) or pre-treated (grey columns) with the drugs indicated on the top of each panel. Neurons were infected with influenza virus strain 24a5b (AIV) or pseudorabies virus strain Yamagata S-81 (PRV). Results are expressed as the percentage of antigen-positive cells in the drug-treated group, with the values of control groups (white columns) adjusted to 100%. In each treatment group, over 400 neurons were examined for the antigen, and the calculation was repeated more than three times using different culture dishes. Asterisk (*), statistically significant difference from untreated controls using the Student's *t*-test ($P<0{\cdot}01$).

for both viruses compared with untreated cells. The morphology of cytoskeletons was not modified by viral infection without drug treatment, and each drug treatment affected the morphology and distribution of only the target cytoskeleton.

DISCUSSION

DRG neurons do not have dendrites *in vivo*, with only a single bifurcating axon and short lateral spikes protruding from the cell body (Thomas *et al.*, 1993). Axons can be distinguished *in vivo* and *in vitro* from other cellular spikes by the presence of MTs and absence of a rough endoplasmic reticulum (Tennyson & Gershon, 1975; Yamada *et al.*, 1971). In our cultures, extensions from neuronal cell bodies were always stained by anti-tubuilin βIII antibody, showing them to be axons. The compartmentalized culture system has been utilized to demonstrate the axonal transport of herpes simplex virus and rabies virus (Lycke & Tsiang, 1987; Ziegler & Herman, 1980), or various biological and biochemical properties of neurons and axons (Campenot, 1977; Hayashi *et al.*, 2004; Kimpinski *et al.*, 1999). The present study with the compartmentalized culture system showed that AIV as well as PRV infecting at the distal part of axons reached neuronal cell bodies through retrograde axonal transport. In our previous papers, we have suggested transneural invasion of intranasally inoculated neurotropic influenza A viruses to the CNS of mice along the peripheral nerves (Matsuda *et al.*, 2004; Park *et al.*, 2002; Shinya *et al.*, 1998, 2000; Tanaka *et al.*, 2003). Several studies of influenza virus infection in brain cell cultures (Brask *et al.*, 2001; Dotti & Simons, 1990; Dotti *et al.*, 1993; Takahashi *et al.*, 1997) or in Schwann cell culture (Levine *et al.*, 2003) have been reported, but the precise mechanisms for the transneural spread of influenza virus, i.e. axonal and transsynaptic transport, have not been characterized. In this paper, using peripheral neurons from neonatal mouse DRG, we demonstrated for the first time the axonal transport of a neurotropic influenza A virus.

The increase in virus antigen-positive neurons in the central chamber of the compartmentalized culture system suggests that AIV as well as PRV spread transsynaptically, since the medium in the chambers contained methyl cellulose for immobilizing viruses and antiserum for neutralizing extracellular-free viruses, and that viruses spreading neuron-to-neuron via synapses are not effectively neutralized by antibodies (Price *et al.*, 1982). The machinery of the transsynaptic spread of influenza virus is unknown. Dotti *et al.* (1993) detected the haemagglutinin antigens at the axonal cell surface but failed to find budding virus from neurons infected with a fowl plague virus by immunoelectron microscopy. A possible explanation might be that the influenza viruses spread as the ribonucleoproteins encompassed in the synaptic vesicles, and that the antiserum cannot prevent the transsynaptic spread of the viruses. The rate of increase in the number of antigen-positive neurons clearly differed between AIV and PRV, and

the result suggests different modes of neuronal propagation for the two viruses, i.e. AIV was transported more promptly within the axons than PRV, and proliferated in the neurons less effectively. There is a possibility that coexisting non-neuronal cells play a substantial role for the virus spread in our culture, but, from the fact that the number of non-neuronal cells was rather small and infected neurons were rarely associated with them, we concluded that transsynaptic spread is likely to be the major cause of the infection of neurons in the central chamber.

There have been many reports concerning virus–cytoskeleton interactions, and MT and associated motor proteins, kinesin and cytoplasmic dynein, play a major role in the transport of internalized viruses to the nucleus (reviewed by Ploubidou & Way, 2001; Sodeik, 2000). However, no information is available on the mechanism of axonal transport of influenza viruses. NOC is a reversible mitotic inhibitor that binds the fast-growing ends of MTs and prevents monomer addition (Cheung & Terry, 1980; Lee *et al.*, 1980). In the present experiments, propagation of PRV was markedly inhibited by NOC treatment. This result was consistent with a previous report that PRV entered neurons by fusing their envelope with the host-cell plasma membrane and their capsid/tegument structure was transported to the nucleus on the MTs by fast axonal transport (Kaelin *et al.*, 2000; Tomishima *et al.*, 2001). The degree of propagation of PRV among the neurons recovered from the NOC treatment was equivalent to the untreated control, indicating that a reconstruction of MTs could afford the effective propagation of the virus. In contrast, the effects of MT disruption by NOC treatment were insignificant for the propagation of AIV. Lakadamyali *et al.* (2003) reported that the incoming transport of influenza A virus strain X-31 (H3N2) to the perinuclear region depends on MTs and dynein-directed motilities in Chinese hamster ovary cells. Whereas, Arcangeletti *et al.* (1997) described independence of influenza virus strain U/73 (H7N1) infection from MT construction in LLC monkey kidney epithelial cells. In the present study, AIV could spread transneurally independent of MTs, whereas the spread of PRV was sensitive to MT inhibition. These results suggest a difference in the mechanism of neuronal spread between these two viruses. However, the enlarged dots of viral antigens in MT-disrupted neurons suggest a significant, but not crucial, effect of MT on the axonal transport of AIV.

MFs and their constituent actin filaments interact with many viruses at various stages throughout their life cycles (reviewed by Cudmore *et al.*, 1997). The most extensively documented viral–actin interactions are those of vaccinia virus, which induces the formation of actin tails that launch viral particles from the cell surface on the tips of microvilli toward neighbouring cells (Cudmore *et al.*, 1995). CYD destabilizes MFs by binding to the fast-growing end of the filaments (Cooper, 1987). With the CYD treatment, the propagation of both AIV and PRV was not obviously affected. PRV has been reported not to interact with MFs (Kaelin *et al.*, 2000; Tomishima *et al.*, 2001), which is consistent with our results. As for influenza virus infection, alternative theories for dependence on actin filaments have been reported. One study emphasized actin-dependent movements of internalized virus during the first step at the cell periphery (Lakadamyali *et al.*, 2003), and another reported that CYD-induced modifications of MFs did not significantly affect influenza virus production (Arcangeletti *et al.*, 1997). From our results, the neuronal spread of AIV was not significantly affected by CYD at the concentration we used. We chose a maximum concentration of CYD not causing detachment of neurons from the floor of the dish based on preliminary experiments. However, it is possible that actin filaments were not sufficiently disrupted at this concentration, and that actin filaments functioned normally for viral propagation.

IFs comprise diverse filamentous proteins characteristically 10–12 nm wide and their distribution is closely related to cell differentiation (reviewed by Coulombe & Wong, 2004). NFs are the major components of IFs in neurons. IFs have long been believed to simply form static 'space filling' cytoplasmic networks and their interactions with viruses are not well documented. Several viral infections have been shown to require intact IF networks using ACR as an IF disruption agent (Eckert, 1985), but very little is known about the roles of the IF network in viral infections (Arcangeletti *et al.*, 1997; Ashok & Atwood, 2003; Cordo & Candurra, 2003). The significant suppression of the spread of AIV and PRV in the ACR-treated cultured neurons infers that intact IF constructions are involved in the transmission of the viruses in the neuronal network. To understand the significant difference in the reduction rate of the infected neurons for both viruses by ACR, however, further experiments for virus-IF interactions are required.

Arcangeletti *et al.* (1997) attributed the dependence of influenza A virus infection on intact IFs to the potential participation of prosomes in viral protein synthesis. Prosomes are ribonucleoprotein particles accompanying untranslated forms of mRNAs (Scherrer & Bey, 1994). Based on their close association with prosomes (Arcangeletti *et al.*, 1992; Olink-Coux *et al.*, 1992), IFs might serve as a network to guide specific prosomes, and possibly mRNAs in the cytoplasm. ACR is a water-soluble vinyl monomer and a well documented neurotoxicant in both humans and laboratory animals (reviewed by LoPachin, 2004). Axonal swelling containing an abundant NFs and degenerating mitochondria have long been considered hallmark lesions produced by the direct action of ACR at axonal or perikaryal sites. However, recent advances in the characterization of ACR neurotoxicity suggest that the nerve terminal is the primary site of ACR action and that inhibition of neurotransmission and membrane turnover in nerve terminals resulting from the ACR-induced disruption of membrane-fusion processes, contributes significantly to the pathogenesis of the neurological defects (LoPachin, 2004; LoPachin *et al.*, 2002). Based on such information, it is conceivable that the

disruption of IFs by ACR suppressed the viral spread by either preventing viral assembly and/or transmisson by IFs, inducing prosome dysfunction or interfering with membrane fusion at synapses.

In conclusion, we demonstrated here, for the first time *in vitro*, the axonal transport of avian influenza virus and MT-independent neuronal propagation of the influenza virus.

ACKNOWLEDGEMENTS

We thank Dr Ichiro Matsuoka, Laboratory of Neuroscience, Graduate School of Pharmaceutical Science, Hokkaido University, and Dr Shuuitsu Tanaka, Molecular Neurobiology Laboratory, Graduate School of Science, Hokkaido University, for providing neuron culture techniques. We are also grateful to Dr Etsuro Ono, Laboratory of Animal Experiment for Disease Model, Institute for Genetic Medicine, Hokkaido University for donating antiserum against pseudorabies virus.

REFERENCES

Arcangeletti, C., Olink-Coux, M., Minisini, R., Huesca, M., Chezzi, C. & Scherrer, K. (1992). Patterns of cytodistribution of prosomal antigens on the vimentin and cytokeratin networks of monkey kidney cells. *Eur J Cell Biol* 59, 464–476.

Arcangeletti, M. C., Pinardi, F., Missorini, S., De Conto, F., Conti, G., Portincasa, P., Scherrer, K. & Chezzi, C. (1997). Modification of cytoskeleton and prosome networks in relation to protein synthesis in influenza A virus-infected LLC-MK2 cells. *Virus Res* 51, 19–34.

Ashok, A. & Atwood, W. J. (2003). Contrasting roles of endosomal pH and the cytoskeleton in infection of human glial cells by JC virus and simian virus 40. *J Virol* 77, 1347–1356.

Brask, J., Owe-Larsson, B., Hill, R. H. & Kristensson, K. (2001). Changes in calcium currents and GABAergic spontaneous activity in cultured rat hippocampal neurons after a neurotropic influenza A virus infection. *Brain Res Bull* 55, 421–429.

Campenot, R. B. (1977). Local control of neurite development by nerve growth factor. *Proc Natl Acad Sci U S A* 74, 4516–4519.

Campenot, R. B. & Martin, G. (2001). Construction and use of compartmented cultures for studies of cell biology of neurons. In *Protocols for Neural Cell Culture*, 3rd edn, pp. 49–57. Edited by S. Fedoroff & A. Richardson. Totowa, NJ: Humana.

Card, J. P., Rinaman, L., Schwaber, J. S., Miselis, R. R., Whealy, M. E., Robbins, A. K. & Enquist, L. W. (1990). Neurotropic properties of pseudorabies virus: uptake and transneuronal passage in the rat central nervous system. *J Neurosci* 10, 1974–1994.

Centers for Disease Control & Prevention (2004). Cases of influenza A (H5N1)-Thailand, 2004. *Morb Mortal Wkly Rep* 53, 100–103.

Cheung, H. T. & Terry, D. S. (1980). Effects of nocodazole, a new synthetic microtubule inhibitor, on movement and spreading of mouse peritoneal macrophages. *Cell Biol Int Rep* 4, 1125–1129.

Claas, E. C. J., Osterhaus, A. D. M. E., van Beek, R., De Jong, J. C., Rimmelzwaan, G. F., Senne, D. A., Krauss, S., Shortridge, K. F. & Webster, R. G. (1998). Human influenza A H5N1 virus related to a highly pathogenic avian influenza virus. *Lancet* 351, 472–477.

Cooper, J. A. (1987). Effects of cytochalasin and phalloidin on actin. *J Cell Biol* 105, 1473–1478.

Cordo, S. M. & Candurra, N. A. (2003). Intermediate filament integrity is required for Junin virus replication. *Virus Res* 97, 47–55.

Coulombe, P. A. & Wong, P. (2004). Cytoplasmic intermediate filaments revealed as dynamic and multipurpose scaffolds. *Nat Cell Biol* 6, 699–706.

Cudmore, S., Cossart, P., Griffiths, G. & Way, M. (1995). Actin-based motility of vaccinia virus. *Nature* 378, 636–638.

Cudmore, S., Rechmann, I. & Way, M. (1997). Viral manipulations of the actin cytoskeleton. *Trends Microbiol* 5, 142–148.

Dotti, C. G. & Simons, K. (1990). Polarized sorting of viral glycoproteins to the axon and dendrites of hippocampal neurons in culture. *Cell* 62, 63–72.

Dotti, C. G., Kartenbeck, J. & Simons, K. (1993). Polarized distribution of the viral glycoproteins of vesicular stomatitis, fowl plague and Semliki Forest viruses in hippocampal neurons in culture: a light and electron microscopy study. *Brain Res* 610, 141–147.

Eckert, B. S. (1985). Alteration of intermediate filament distribution in PtK1 cells by acrylamide. *Eur J Cell Biol* 37, 169–174.

Enquist, L. W., Tomishima, M. J., Gross, S. & Smith, G. A. (2002). Directional spread of an α-herpesvirus in the nervous system. *Vet Microbiol* 86, 5–16.

Field, H. J. & Hill, T. J. (1974). The pathogenesis of pseudorabies in mice following peripheral inoculation. *J Gen Virol* 23, 145–157.

Frankova, V., Jirasek, A. & Tumova, B. (1977). Type A influenza: postmortem virus isolations from different organs in human lethal cases. *Arch Virol* 53, 265–268.

Hakoda, S. & Nakatani, T. (2000). A pregnant woman with influenza A encephalopathy in whom influenza A/Hong Kong virus (H3) was isolated from cerebrospinal fluid. *Arch Intern Med* 160, 1041–1045.

Hayashi, H., Campenot, R. B., Vance, D. E. & Vance, J. E. (2004). Glial lipoproteins stimulate axon growth of central nervous system neurons in compartmented cultures. *J Biol Chem* 279, 14009–14015.

Itakura, C., Nakatsuka, J. & Goto, M. (1981). An incidence of pseudorabies (Aujeszky's disease) in piglets in Japan. *Nippon Juigaku Zasshi* 43, 923–927.

Ito, T., Goto, H., Yamamoto, E., Tanaka, H., Takeuchi, M., Kuwayama, M., Kawaoka, Y. & Otsuki, K. (2001). Generation of a highly pathogenic avian influenza A virus from an avirulent field isolate by passaging in chickens. *J Virol* 75, 4439–4443.

Kaelin, K., Dezélée, S., Masse, M. J., Bras, F. & Flamand, A. (2000). The UL25 protein of pseudorabies virus associates with capsids and localizes to the nucleus and to microtubules. *J Virol* 74, 474–482.

Kida, H., Yanagawa, R. & Matsuoka, Y. (1980). Duck influenza lacking evidence of disease signs and immune response. *Infect Immun* 30, 547–553.

Kida, H., Kawaoka, Y., Naeve, C. W. & Webster, R. G. (1987). Antigenetic and genetic conservation of H3 influenza virus in wild ducks. *Virology* 159, 109–119.

Kimpinski, K., Jelinski, S. & Mearow, K. (1999). The anti-p75 antibody, MC192, and brain-derived neurotrophic factor inhibit nerve growth factor-dependent neurite growth from adult sensory neurons. *Neuroscience* 93, 253–263.

Lakadamyali, M., Rust, M. J., Babcock, H. P. & Zhuang, X. (2003). Visualizing infection of individual influenza viruses. *Proc Natl Acad Sci U S A* 100, 9280–9285.

Lee, J. C., Field, D. J. & Lee, L. L. (1980). Effects of nocodazole on structures of calf brain tubulin. *Biochemistry* 19, 6209–6215.

Levine, J., Buchman, C. A. & Fregien, N. (2003). Influenza A virus infection of human Schwann cells in vitro. *Acta Otolaryngol* 123, 41–45.

LoPachin, R. M. (2004). The changing view of acrylamide neurotoxicity. *Neurotoxicology* 25, 617–630.

LoPachin, R. M., Ross, J. F. & Lehning, E. J. (2002). Nerve terminals as the primary site of acrylamide action: a hypothesis. *Neurotoxicology* 23, 43–59.

Lycke, E. & Tsiang, H. (1987). Rabies virus infection of cultured rat sensory neurons. *J Virol* **61**, 2733–2741.

Matsuda, K., Park, C. H., Sunden, Y., Kimura, T., Ochiai, K., Kida, H. & Umemura, T. (2004). The vagus nerve is one route of transneural invasion for intranasally inoculated influenza A virus in mice. *Vet Pathol* **41**, 101–107.

Mounts, A. W., Kwong, H., Izurieta, H. S. & 10 other authors (1999). Case-control study of risk factors for avian influenza A (H5N1) disease, Hong Kong, 1997. *J Infect Dis* **180**, 505–508.

Olink-Coux, M., Huesca, M. & Scherrer, K. (1992). Specific types of prosomes are associated to subnetworks of the intermediate filaments in PtK1 cells. *Eur J Cell Biol* **59**, 148–159.

Park, C. H., Ishinaka, M., Takada, A., Kida, H., Kimura, T., Ochiai, K. & Umemura, T. (2002). The invasion routes of neurovirulent A/Hong Kong/483/97 (H5N1) influenza virus into the central nervous system after respiratory infection in mice. *Arch Virol* **147**, 1425–1436.

Ploubidou, A. & Way, M. (2001). Viral transport and the cytoskeleton. *Curr Opin Cell Biol* **13**, 97–105.

Price, R. W., Rubenstein, R. & Khan, A. (1982). Herpes simplex virus infection of isolated autonomic neurons in culture: viral replication and spread in a neuronal network. *Arch Virol* **71**, 127–140.

Scherrer, K. & Bey, F. (1994). The prosomes (multicatalytic proteinases; proteasomes) and their relationship to the untranslated messenger ribonucleoproteins, the cytoskeleton, and cell differentiation. *Prog Nucleic Acid Res Mol Biol* **49**, 1–64.

Shinya, K., Silvano, F. D., Morita, T., Shimada, A., Nakajima, M., Ito, T., Otsuki, K. & Umemura, T. (1998). Encephalitis in mice inoculated intranasally with an influenza virus strain originated from a water bird. *J Vet Med Sci* **60**, 627–629.

Shinya, K., Shimada, A., Ito, T., Otsuki, K., Morita, T., Tanaka, H., Takada, A., Kida, H. & Umemura, T. (2000). Avian influenza virus intranasally inoculated infects the central nervous system of mice through the general visceral afferent nerve. *Arch Virol* **145**, 187–195.

Silvano, F. D., Yoshikawa, M., Shimada, A., Otsuki, K. & Umemura, T. (1997). Enhanced neuropathogenicity of avian influenza A virus by passages through air sac and brain of chicks. *J Vet Med Sci* **59**, 143–148.

Sodeik, B. (2000). Mechanisms of viral transport in the cytoplasm. *Trends Microbiol* **8**, 465–472.

Takahashi, M., Yamada, T., Nakanishi, K., Fujita, K., Nakajima, K., Nobusawa, E., Yamamoto, T., Kato, T. & Okada, H. (1997). Influenza A virus infection of primary cultured cells from rat fetal brain. *Parkinsonism Relat Disord* 3, 97–102.

Tanaka, H., Park, C. H., Ninomiya, A., Ozaki, H., Takada, A., Umemura, T. & Kida, H. (2003). Neurotropism of the 1997 Hong Kong H5N1 influenza virus in mice. *Vet Microbiol* **95**, 1–13.

Tennyson, V. M. & Gershon, M. D. (1975). Light and electron microscopy of dorsal root, sympathetic, and enteric ganglia. In *Peripheral Neuropathy*, 2nd edn, vol. 1, 121–155. Edited by P. J. Dyck, P. K. Thomas, J. W. Griffin, P. A. Low & J. F. Poduslo. London: Saunders.

Thomas, P. K., Berthold, C. H. & Ochoa, J. L. (1993). Microscopic anatomy of the peripheral nervous system. In *Peripheral Neuropathy*, 3rd edn, vol. 1, pp. 28–91. Edited by P. J. Dyck, P. K. Thomas, J. W. Griffin, P. A. Low & J. F. Poduslo. London: Saunders.

Togashi, T., Matsuzono, Y., Anakura, M. & Nerome, K. (1997). Acute encephalitis and encephalopathy at the height of influenza in childhood. *Nippon Rinsho* 55, 2699–2705.

Tomishima, M. J., Smith, G. A. & Enquist, L. W. (2001). Sorting and transport of alpha herpesviruses in axons. *Traffic* 2, 429–436.

Tran, T. H., Nguyen, T. L., Nguyen, T. D. & 27 other authors (2004). Avian influenza A (H5N1) in 10 patients in Vietnam. *N Engl J Med* **350**, 1179–1188.

Turner, D., Wailoo, A., Nicholson, K., Cooper, N., Sutton, A. & Abrams, K. (2003). Systematic review and economic decision modelling for the prevention and treatment of influenza A and B. *Health Technol Assess* 7, 1–182.

Webster, R. G., Bean, W. J., Gorman, O. T., Chambers, T. M. & Kawaoka, Y. (1992). Evolution and ecology of influenza A viruses. *Microbiol Rev* **56**, 152–179.

Yamada, K. M., Spooner, B. S. & Wessells, N. K. (1971). Ultrastructure and function of growth cones and axons of cultured nerve cells. *J Cell Biol* **49**, 614–635.

Yuen, K. Y., Chan, P. K. S., Peiris, M. & 8 other authors (1998). Clinical features and rapid viral diagnosis of human disease associated with avian influenza A H5N1 virus. *Lancet* **351**, 467–471.

Ziegler, R. J. & Herman, R. E. (1980). Peripheral infection in culture of rat sensory neurons by herpes simplex virus. *Infect Immun* **28**, 620–623.

Available online at www.sciencedirect.com
SCIENCE DIRECT®
Biosensors and Bioelectronics 21 (2005) 201–205
BIOSENSORS & BIOELECTRONICS
www.elsevier.com/locate/bios

Short communication

Application of carbon nanotubes for detecting anti-hemagglutinins based on antigen–antibody interaction

Seiji Takeda[a,*], Agus Sbagyo[a], Yoshihiro Sakoda[b], Atsushi Ishii[c], Makoto Sawamura[d], Kazuhisa Sueoka[a], Hiroshi Kida[b], Koichi Mukasa[a], Kazuhiko Matsumoto[e]

[a] *Graduate School of Engineering, Hokkaido University, Kita 13 Nishi 8 Kita-ku, Sapporo 060-8628, Japan*
[b] *Graduate School of Verterinary, Department of Disease Control, Hokkaido University, Kita 18 Nishi 9 Kita-ku, Sapporo 060-0818, Japan*
[c] *Creative Research Initiative "Sousei" Hokkaido University, Kita 21 Nishi 10 Kita-ku, Sapporo 001-0021, Japan*
[d] *Innovation Plaza Hokkaido, Japan Science and Technology Agency, Kita 19 Nishi 11 Kita-ku, Sapporo 060-0819, Japan*
[e] *The Institute of Scientific and Industrial Research, Osaka University, 8-1 Mihogaoka, Ibaraki, Osaka 567-0047, Japan*

Received 10 May 2004; received in revised form 18 June 2004; accepted 23 August 2004
Available online 2 October 2004

Abstract

Carbon nanotube sensors detected anti-hemagglutinin binding to immobilized hemagglutinins. An ultra-sensitive detection method for antibodies or antigens in serum is required. Hemagglutinins were immobilized on the reverse side of a carbon nanotube, thereby producing a source and a drain. Electrode pads covered each edge of the nanotube. The *I–V* curves between the source and the drain were measured after incubation of anti-hemagglutinins with immobilized hemagglutinins in a buffered solution on the reverse side of the nanotube. The sensitivity of the CNT sensor was higher than that of an ELISA system. This method constitutes a new tool to analyze interaction among biomolecules on a substrate.

Keywords: Carbon nanotubes; Anti-hemagglutinin; Antigen–antibody interaction

1. Introduction

A sensitive detection method is required for some viruses, specific antibodies, metabolized materials, and heavy metal ions in serum or body fluid. Such a method would not just facilitate the examination of blood for transfusions or be used in evaluating environmental pollution, but also aid in the investigation of the binding processes of biomolecules while using small sample amounts. Sensitivity and size of equipment are crucial factors for biosensors, especially for outdoor use.

Sensors based on field effect transistors (FETs) are also useful for ion-sensitive electrodes or biosensors (Bergveld, 1970; Korpan et al., 2000; Ingebrandt et al., 2003). Miniaturization of FETs is easier than an enzyme-linked immunosorbent assay (ELISA) or the polymerase chain reaction (PCR) method. Several such devices are commercially available. An advantage of this method is that it requires only a few tens of milliseconds to measure one sample. Moreover, the sensors can be small and can test a number of samples simultaneously. Tsuruta reported an ELISA system using a pH-FET or an ion-selective FET to improve the detection limit of ELISA (Tsuruta et al., 1994, 1995).

Tans et al. demonstrated the possibility of using an individual semiconducting single-walled carbon nanotube (SWCNT) as an FET transistor (Tans et al., 1998). Chemical sensors based on carbon nanotubes have recently attracted a great deal of attention (Besteman et al., 2003; Chen et al., 2004; Collins et al., 2003; Someya et al., 2003). Nanotubes are expected to exhibit excellent properties as transducers. Moreover, they are ideal material for ultra-small sensors because they have a large surface area and are known to exhibit charge-sensitive conductance. Semiconducting SWCNTs have high mobility; all their atoms are located on the surface.

* Corresponding author. Tel.: +81 11 703 7179; fax: +81 11 706 7803.
E-mail address: takeda@nano.eng.hokudai.ac.jp (S. Takeda).

0956-5663/$ – see front matter © 2004 Elsevier B.V. All rights reserved.
doi:10.1016/j.bios.2004.08.030

Protein sensors based on carbon nanotubes were reported by Star et al. (2003). They established that interaction between biotin and streptavidin on CNT is detectable by measuring I–V_{gate} curves. Their study showed that the biotin moiety was absorbed irreversibly on the CNT wall. They observed the binding of streptavidin to biotin immobilized on the CNT-FET sensors. Even though the effect of the interaction on the FET signal is greater in direct modification of the CNT than in modification on the reverse side, it is sometimes difficult to recover the CNT after the reaction by washing. The present study immobilizes hemagglutinins (HA), which are influenza virus membrane proteins, on the reverse side of the CNT sensors. In this case, strong chemicals can be used to remove the protein, thereby lengthening the CNT lifetime because the reaction takes place on the reverse side of the CNT. In this manner, we demonstrate that the CNT sensor shows higher sensitivity than ELISA in detecting the binding of anti-HA to HA.

2. Materials and method

N-[5-(3′-Maleimidopropylamido)-1-carboxypentyl]iminodiacetic acid, disodium salt, and monohydrate (Maleimide NTA) were purchased from Dojindo Laboratories, Japan. 3-Mercaptopropyltriethoxysilane (S810) was purchased from Chisso Corp., Japan. Other materials were purchased from Sigma–Aldrich Co., Japan.

2.1. Growth of CNT on a silicon surface

The CNT-FET device was fabricated by a combination of position-controlled growth of CNTs, electron beam lithography (EBL), and electron beam (EB) deposition.

2.1.1. Formation of the chemical catalyst

An Si (0 0 1) substrate with a thermally grown SiO_2 has been used as a substrate. The thickness of SiO_2 was 300 nm. Firstly, a polymethylmethacrylate (PMMA) film was formed on the substrate by spin coating. Pairs of round-shaped holes with a diameter of 3 μm and a spacing of 3 μm were fabricated in the PMMA film using EBL. After depositing a 10 nm-thick Si film and a 10 nm-thick Mo film, a 3 nm-thick Fe film was deposited on the patterned substrate by means of EB deposition. After the PMMA film was stripped, ordered pairs of round-shaped catalyst patterns were obtained.

2.1.2. CNT growth

The SWCNTs were grown by means of the chemical vapor deposition (CVD; Easy Tube CO.) method. The patterned substrate was heated up to 900 °C in the tube furnace under argon flow (at the rate of 1000 sccm). After reaching 900 °C, the argon gas was replaced by methane (1000 sccm) and hydrogen (500 sccm) in order to grow the SWCNTs. Hydrogen gas was used to purify the SWCNTs. The growth time was 10 min. After growth, the furnace was cooled to room temperature in an argon atmosphere.

2.1.3. Deposition of metallic electrodes

The patterns for formation of metallic electrodes were fabricated using the same process as that used in the formation of the chemical catalyst. For the metallic electrodes, a 30 nm-thick Pt film and a 100 nm-thick Au film were deposited using EB deposition. The electrodes covered the chemical catalyst and had a spacing of 2 μm.

2.2. Hemagglutinin protein and monoclonal antibody of the influenza A virus

The hemagglutinin gene of the influenza virus A/swine/Hong Kong/10/98 (H9N2) was amplified by RT-PCR. The amplified gene was cloned into the mammalian expression vector pCAGGS/MCS (Niwa and Yamamura, 1991). Then, this construct was transfected into 293T cells for the expression of the recombinant hemagglutinin protein. The cytoplasmic lysate of this transfected cell was extracted and the expressed hemagglutinin protein was purified by Ni^{2+} affinity chromatography (Amersham Biosciences, USA) and dialyzed in phosphate buffered saline (PBS). Monoclonal antibody E2/3 against hemagglutinin of A/swine/Hong Kong/10/98 (H9N2) was produced according to the protocol by Kida et al. (1982). The concentration of HA and anti-HA were determined as 1.929 and 5.125 mg/ml, respectively.

2.2.1. ELISA

ELISA plates were coated with HA. The anti-HA was diluted from 5.12×10^{-2} to 1.25×10^{-5} mg/ml. Diluted anti-HA was absorbed on an ELISA plate. The anti-mouse IgG that carried horse radish peroxidase (HRPO) was incubated after rinsing the plate. The HRPO can convert the light-absorbing 3,3′,5,5′-tetramethylbenzidine at approximately 450 nm. Instead of the anti-HA, only a buffer was used as a control experiment. The absorbance at 450 nm of the control experiment was 0.076. The absorbance of each diluted sample of 450 nm were measured after stopping the HRPO reaction.

2.3. Modification of the reverse side of the CNT

The reverse side of the CNT was washed and cleaned with ethanol and 10% H_2SO_4 before modification in order to obtain an oxidized surface. After heating the surface at 180 °C for 1 h, S810 was dropped on the substrate and a cover glass was used to cover the area. Following this, heating was resumed for a minimum of 2 h at 180 °C. Dithiothreitol (50 mM) was dropped onto the surface at 30 °C for 12 h. After washing away dithiothreitol with pure water, 1 mg/ml maleimide NTA was reacted with the thiol group of S810 that was immobilized on the substrate for 1 h at room temperature. Next, 50 mM NiCl was dropped on the surface and incubated

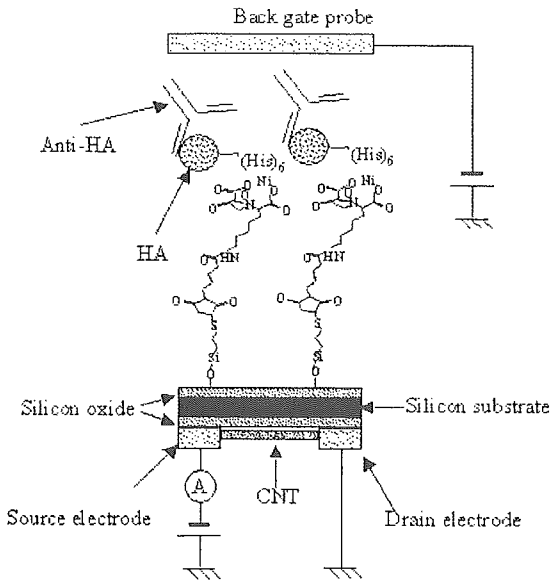

Fig. 1. *I–V* curves of CNT with and without biomolecule immobilization. (a) Schematic model of *I–V* measurement using the CNT sensors. The *I–V* curves were measured in air and −20 V was applied to the back gate. (b) A set of *I–V* curves without modification. Thick solid, thin solid, thick dotted, and thin dotted lines represent data obtained after application of −20, −15, −10, and −5 V to the back gates of the respective CNTs.

for 15 min after washing away unreacted maleimide NTA with pure water. Next, 1.929 μg/ml HA was dropped on the surface for 15 min at 25 °C. After washing with the buffer and pure water, 10 μl of various concentrations of anti-HA, from 5.12×10^{-10} to 5.12×10^{-5} mg/ml, were dropped onto the surface for 15 min at 25 °C. The I–V_{sd} curves were measured at each step of the reaction between HA and anti-HA after drying the surface with nitrogen gas.

2.4. *I–V* measurements

In order to examine the properties of CNT, the current between the source and drain (I_{sd}) was measured in air by applying 0 to −20 V to the back gate that faced the reverse side of the CNTs. The schematic model of the *I–V* measurements is shown in Fig. 1. The I_{sd} was plotted as a function of the potential between the source and drain (*I–V* curve). A Keithley 4200 semiconductor characterization system was employed to measure the *I–V* curves at room temperature.

3. Results and discussion

We investigated the properties of the CNT grown on the substrate by measuring the I–V_{sd} curves while changing the potential of the reverse side of the CNT sensors by employing the back gate potential control system. The I_{sd} was dependent on the potential of the back gate, as in an FET device (data not shown). The FET property of a CNT is not consistent with that reported elsewhere by Bradley et al. (2003). The CNT showed conductive or semiconductive properties depending on the CNT chirality. In this experiment, I_{sd} increased when the back gate potential decreased to −20 V, suggesting that I_{sd} was strongly affected by the effective potential around the CNT. The *I–V* curves were measured before and after the addition of anti-HA while applying −20 V to the back gate because the CNT response was the greatest for the *I–V* curves.

HA was designed to produce a complex with the Ni cation by attaching a histidine tag at the C terminus of the HA. The histidine tag method was reported by Hochuli et al. (1987). It was used to control the orientation of the immobilized protein or peptide (Schmid et al., 1997; Rigler et al., 2003). The *I–V* curves are shown in Fig. 2a before and after addition of anti-HA to HA immobilized on the surface by the histidine tag. In this case, HA and anti-HA could interact and bind on the reverse side of the CNT sensor. We showed only those *I–V* curves in the 0–1.5 V range of V_{sd} because the change effected by the antigen and antibody in this range was clearer than that in the other ranges. After the addition of HA, I_{sd} decreased between 1 and 1.5 V of V_{sd}. This decrease suggested that the effective potential around CNT might change to positive by producing a complex between HA and Ni cation. The I_{sd} between 1 and 1.5 V of V_{sd} increased along with an increase in the concentration of the anti-HA.

Fig. 2b shows the *I–V* curves before and after addition of anti-HA without HA immobilization as a control experiment. In this case, only non-specific binding of anti-HA to the sensor surface would be observed. Fig. 2b was obtained before measuring Fig. 2a using the same CNT sensor. In Fig. 2b, I_{sd} did not increase after addition of the anti-HA and so there was no clear correlation between I_{sd} and the concentration of anti-HA as indicated in Fig. 2a. The error of measurement of each reaction process was estimated to be less than 1 μA, which is deduced from the *I–V* curve noise. The increase of the I_{sd} phenomena from 1 to 1.5 V seemed uncharacteristic if only one SWCNT was connected between the electrode pads. One possible explanation is that there was more than one CNT grown between the electrodes whose properties were different. Another possible explanation is the existence of the binding junction between the CNT and the electrode, i.e., the kink effect. The change in diameter of the CNT also complicates the *I–V* curves. Further studies are required to investigate the properties of the CNT and CNT sensors. This result suggests that the increase of I_{sd}, as depicted in Fig. 2a, resulted from specific binding of anti-HA to the immobilized HA and that the binding might have changed the effective potential around the CNT to negative.

The I_{sd} at 1.5 V for the *I–V* curves is plotted in Fig. 2c. The closed and open circles show results from Fig. 2a and b, respectively. Fig. 2c clearly shows that the I_{sd} increased from 2.3 to 4.2 μA with an increase in the concentration of the anti-HA from 5.12×10^{-8} to 5.12×10^{-6} mg/ml. Control experiments (open circle) appear to indicate that I_{sd} was in the range of 1.5–2.5 μA as a result of the measurement error

and non-specific binding of anti-HA to the substrate surface. The line drawn on the closed circle in Fig. 2c is the tentative calibration line of the CNT sensor. The detection limit of anti-HA using the CNT sensor was estimated to be approximately 5×10^{-8} mg/ml from the tentative calibration line.

We also used ELISA to examine the anti-HA detection limit. Instead of the anti-HA, only buffer was used as a control experiment. A stock solution of the anti-HA was diluted from 5.12×10^{-2} to 1.25×10^{-5} mg/ml. The closed triangle in Fig. 2c shows the absorbance at 450 nm, measured after stopping the HRPO reaction. In this case, absorbance increased along with an increase in the concentration of anti-HA from 1×10^{-4} to 1×10^{-3} mg/ml. From the results, the detection limit using ELISA was estimated to be 5.0×10^{-5} mg/ml, taking the absorbance of the sample to be the same as the average absorbance of the control experiment plus five times the standard deviation. The line drawn on the closed triangle in Fig. 2c is a tentative calibration line according to the ELISA method.

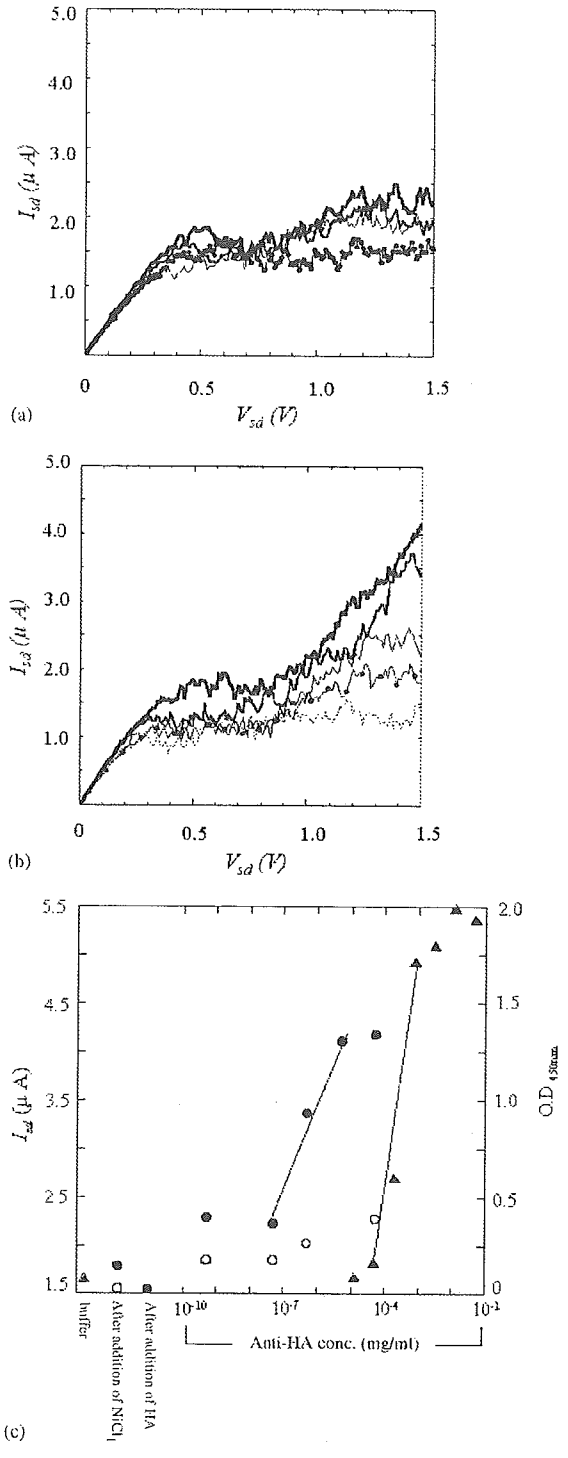

As shown in Fig. 2c, the sensitivity of the CNT base on FET was at least 10 times higher than that using ELISA in the case of anti-HA detection using the CNT sensor. We also examined the effect of anti-HA binding to HA on the I–V curves using other CNT sensors. The detection limit of these was not the same in both cases. However, the same phenomenon, i.e., the increase in I_{sd} after the addition of anti-HA to the HA immobilized surface, was observed in each case (data not shown). The sensitivities of these sensors were higher than or almost similar to those for the ELISA method. The difference in the properties of each of the CNT sensors seems to contribute to the difference in the detection limits. As CNTs are known to exhibit charge-sensitive conductance, the detection limit of the antigens or antibodies will depend on the kind of antibody or the electronic density of the antibody surface. Detection of the interaction of hydrophilic proteins, ion-binding proteins, and DNA can be performed with high sensitivity because they usually have an electronic charge on the surface.

4. Conclusion

The detection limit of anti-HA using the CNT sensor was estimated to be 5×10^{-8} mg/ml from the tentative calibration line of the CNT sensor, whereas the detection limit of anti-HA using ELISA was estimated to be 5.0×10^{-5} mg/ml. This contrast implies that the CNT sensor has the potential to detect HA by this method with higher sensitivity than by the ELISA method, although the sensitivities depend on the CNT

Fig. 2. Detection of the binding of anti-HA to immobilized HA using the CNT sensor. (a) Effect of the binding of anti-HA to immobilized HA on the I–V curves. Thin lines with closed circles and dotted lines represent data obtained after the addition of $NiCl_2$ and HA, respectively. Solid, semi-thick, and thick lines represent data obtained after the addition of 5.125×10^{-8}, 5.125×10^{-7}, and 5.125×10^{-5} mg/ml of anti-HA, respectively. (b) Effect of non-specific binding of anti-HA to the surface on the I–V curves. The solid line with closed circles represents data obtained after the addition of $NiCl_2$. The solid, semi-thick, and thick lines represent data obtained after addition of 5.125×10^{-8}, 5.125×10^{-7}, and 5.125×10^{-5} mg/ml of anti-HA, respectively. (c) Current (I_{sd}) is plotted at 1.5 V of the I–V curves. The closed circles and open circles represent data obtained with and without anti-HA immobilization, respectively. The closed triangle represents absorbance at 450 nm, measured after stopping the HRPO reaction.

sensors. This study also suggests that the method might be applicable for the detection of other antigen and antibody reactions, or any interactions between biomolecules. Nevertheless, further investigation regarding CNT sensor properties is required.

Acknowledgements

This work was supported by Core Research for Evolutional Science and Technology (CREST) of the Japan Science and Technology Corporation (JST).

References

Bergveld, P., 1970. Development of an ion-sensitive solid-state device for neurophysiological measurents. IEEE Trans. BME 17, 70–71.

Besteman, K., Lee, J.-O., Wiertz, F.G.M., Heering, H.A., Dekker, C., 2003. Enzyme-coated nanotubes as single-molecule biosensors. Nano Lett. 3, 727–730.

Bradley, K., Cumings, J., Star, A., Gabriel, J.-C.P., Gruner, G., 2003. Influence of mobile ions on nano tube based FET devices. Nano Lett. 3 (5), 639–641.

Chen, R.J., Choi, H.C., Bangsaruntip, S., Yenilmez, E., Tang, X., Wang, Q., Chang, Y.L., Dai, H., 2004. An investigation of the mechanisms of electronic sensing of protein adsorption on carbon nanotube devices. J. Am. Chem. Soc. 126, 1563–1568.

Collins, P.G., Bradlley, K., Ishigami, M., Zettl, A., 2000. Extreme oxygen sensitivity of electronic properties of carbon nanotubes. Science 287, 1801–1804.

Hochuli, E., Doeli, H., Schacher, A., 1987. New metal chelate adsorbent selective for proteins and peptides containing neighbouring histidine residues. J. Chromatogr. 411, 177–184.

Ingebrandt, S., Yeung, C.K., Staag, W., Zettere, T., Offenhausser, A., 2003. Backside contacted field effect transistor array for extracellular signal recording. Biosens. Bioelectron. 18, 429–435.

Kida, H., Brown, L.E., Webster, R.G., 1982. Biological activity of monoclonal antibodies to operationally defined antigenic regions on the hemagglutinin molecule of A/Seal/Massachusetts/1/80 (H7N1) influenza virus. Virology 122 (1), 38–47.

Korpan, Y.I., Gonchar, M.V., Sibirny, A.A., Martelet, C., El'skaya, A.V., Gibson, T.D., Soldatkin, A.P., 2000. Development of highly selective and stable potentiometric sensors for formaldehyde determination. Biosens. Bioelectron. 15, 77–83.

Niwa, H., Yamamura, K., 1991. Efficient selection for high-expression transfectants with a novel eukaryotic vector. Gene 15, 108 (2), 193–199.

Rigler, P., Ulrich, W.P., Hoffmann, P., Mayer, M., Vogel, H., 2003. Reversible immobilization of peptides: surface modification and in situ detection by attenuated total reflection FTIR spectroscopy. Chem. Phys. Chem. 4, 268–275.

Schmid, E.L., Keller, T.A., Dienes, Z., Vogel, H., 1997. Reversible oriented surface immobilization of functional proteins on oxide surface. Anal. Chem. 69, 1979–1985.

Someya, T., Small, J., Kim, P., Nuckolls, C., Yardley, J.T., 2003. Alcolol vapor sensors based on single-walled carbon nanotube field effect transistors. Nano Lett. 3 (7), 877–881.

Star, A., Gabriel, J.-C.P., Bradley, K., Gruner, G., 2003. Electronic detection of specific protein binding using nanotube FET devices. Nano Lett. 3 (4), 459–463.

Tans, S.J., Verschueren, A.R.M., Dekker, C., 1998. Room-temperature transistor based on a single carbon nanotube. Nature 393, 49–52.

Tsuruta, H., Matsui, S., Hatanaka, T., Namba, T., Miyamoto, K., Nakamura, M., 1994. Detection of the products of polymerase chain reaction by an ELISA system based on an ion sensitive field effect transistor. J. Immunol. Methods 176, 45–52.

Tsuruta, H., Yamada, H., Motoyashiki, Y., Oka, K., Okada, C., Nakamura, M., 1995. An automated ELISA system using a pipette tip as a soloid phase and a pH-sensitive field effect transistor as adetector. J. Immunol. Methods 183, 221–229.

Microbiol. Immunol., 49(12), 1063–1067, 2005

Editor-Communicated Paper

Evaluation of the ESPLINE® INFLUENZA A&B-N Kit for the Diagnosis of Avian and Swine Influenza

Gui-Rong Bai[1], Yoshihiro Sakoda[1], Aaron Simanyengwe Mweene[1], Noriko Kishida[1], Takashi Yamada[2], Hidetaka Minakawa[2], and Hiroshi Kida*[,1]

[1]*Department of Disease Control, Graduate School of Veterinary Medicine, Hokkaido University, Sapporo, Hokkaido 060–0818, Japan, and* [2]*Fujirebio, Inc., Hachioji, Tokyo 192–0031, Japan*

Communicated by Dr. Kazumasa Ogasawara: Received September 20, 2005. Accepted September 30, 2005

***Abstract*: The ESPLINE® INFLUENZA A&B-N kit was evaluated for its applicability to the rapid diagnosis of influenza in chickens and pigs. The kit specifically detected viral antigens in tracheal swabs and tissue homogenates of the trachea, liver, spleen, and colon of chickens inoculated with a highly pathogenic avian influenza virus strain, A/chicken/Yamaguchi/7/04 (H5N1), at 48 hr post-inoculation (p.i.) as well as in the tracheal and cloacal swabs and tissue homogenates of dead chickens. For those infected with a low pathogenic strain, A/chicken/aq-Y-55/01 (H9N2), antigens were detected only in the samples from tracheal swabs and organs 1–4 days p.i. The kit also detected viral antigens in the nasal swabs of miniature pigs infected with swine and avian influenza viruses. The kit was found to be sensitive and specific enough for the rapid diagnosis of infections of influenza A virus in chickens and pigs.**

***Key words*: Animal experiment, Influenza, Rapid diagnosis**

Influenza, caused by type A influenza viruses of 15 or possibly 16 (9) haemagglutinin (HA) and 9 neuraminidase subtypes (1), yields significant mortality and morbidity in domestic poultry, pigs, and horses as well as in humans throughout the world (20). Some strains of subtype H5 or H7 cause highly pathogenic avian influenza (HPAI) in chickens, a systemic infection in which mortality ranges from 75 to 100%. In avian species, most infections cause a mild disease known as low pathogenic avian influenza (LPAI). The LPAI viruses H1–H15, particularly H9N2 and H6N2, have caused outbreaks of disease worldwide with high morbidity in poultry and are still in circulation (1, 5, 11). Swine influenza viruses H1N1, H1N2, and H3N2 have been shown to be endemic in North America, South America, Europe, and Asia. Pigs infected with these viruses may develop apparent clinical signs that include anorexia, inactivity, prostration, difficulty in breathing, coughing, fever, conjunctivitis, rhinitis, and sneezing (4). The potential for avian influenza viruses of all HA subtypes to infect pigs has been demonstrated (10).

**Address correspondence to* Dr. Hiroshi Kida, Department of Disease Control, Graduate School of Veterinary Medicine, Hokkaido University, Kita 18, Nishi 9, Kita-ku, Sapporo, Hokkaido 060–0818, Japan. Fax: +81–11–706–5273. E-mail: kida@vetmed.hokudai.ac.jp

Early detection of the influenza virus in infected animals would improve the control of influenza. Rapid immunological tests and the reverse transcription polymerase chain reaction (RT-PCR) have been used to detect influenza viruses in throat and nasal specimens collected from humans, pigs, and horses (3, 6, 16, 17). The rapid and accurate detection of influenza viruses is of significant importance in animal influenza monitoring and control programmes. The ESPLINE® INFLUENZA A&B-N is a rapid diagnostic kit to detect nucleoproteins (NP) of influenza A and B viruses (2). In the present study, we evaluated the suitability of this kit for the rapid detection of antigens in chickens and pigs infected experimentally with influenza A viruses.

Materials and Methods

ESPLINE® INFLUENZA A&B-N. The immunochromatography and enzyme immunoassay kit was evaluat-

Abbreviations: APMV, avian paramyxovirus; BSL 3, biosafety containment level III; Dk, duck; EID_{50}, 50% egg infectious dose; HA, haemagglutinin; HPAI, highly pathogenic avian influenza; LPAI, low pathogenic avian influenza; MDCK, Madin-Darby canine kidney cell; NP, nucleoprotein; p.i., post-inoculation; RT-PCR, reverse transcription polymerase chain reaction; SPF, specific pathogen-free; Sw, swine; $TCID_{50}$, 50% tissue infectious dose.